

Multi-Site rs-fMRI Domain Alignment for Autism Spectrum Disorder Auxiliary Diagnosis Based on Hyperbolic Space

Yiqian Luo, Qiurong Chen, Yangsong Zhang

Abstract—In the medical field, most resting-state fMRI (rs-fMRI) data are collected from multiple hospital sites. Multi-site rs-fMRI data can increase the volume of training data, enabling auxiliary diagnostic algorithms for brain diseases to learn more accurate and stable models. However, due to the significant heterogeneity and domain shift in rs-fMRI data across different sites, the accuracy of auxiliary diagnosis remains unsatisfactory. Moreover, there has been limited exploration of multi-source domain adaptation algorithms, and the interpretability of models is often poor. To address these challenges, we proposed a domain-adaptive algorithm based on hyperbolic space embedding. Hyperbolic space is naturally suited for representing the topology of complex networks such as brain functional networks. Therefore, we embedded the brain functional network into hyperbolic space and constructed the corresponding hyperbolic space community network to effectively extract brain network representations. To address the heterogeneity of data across different sites and the issue of domain shift, we introduce a constraint loss function, HMMD (Hyperbolic Maximum Mean Discrepancy), to align the marginal distributions in the hyperbolic space. Additionally, we employ class prototype alignment to align the conditional distributions. This significantly improves the quality of brain representations and enhances diagnostic classification accuracy for Autism Spectrum Disorder (ASD). Experimental results demonstrated that the proposed algorithm is robust to multi-site heterogeneity and shows promising potential for brain network mechanism analysis.

Index Terms—rs-fMRI, Autism spectrum disorder, Multi-site domain adaptation, Graph convolution, hyperbolic space, Functional gradients, Prototype learning

I. INTRODUCTION

Autism Spectrum Disorder (ASD) is a widespread developmental disorder that affects approximately 1% of the population [1], severely disrupting daily life and being

This paragraph of the first footnote will contain the date on which you submitted your paper for review. It will also contain support information, including sponsor and financial support acknowledgment. For example, “This work was supported in part by the U.S. Department of Commerce under Grant 123456.”

The next few paragraphs should contain the authors’ current affiliations, including current address and e-mail. For example, First A. Author is with the National Institute of Standards and Technology, Boulder, CO 80305 USA (e-mail: author@boulder.nist.gov).

The authors are with the Laboratory for Brain Science and Artificial Intelligence, School of Computer Science and Technology, Southwest University of Science and Technology, Mianyang, China (e-mail: yiqian-luo_academy@163.com).

associated with a high prevalence of comorbid conditions such as depression and anxiety [2]. ASD typically emerges in childhood, with lifelong symptoms that often require long-term support [3]. The main characteristics of ASD include social communication deficits and restricted, repetitive behaviors, with severity ranging from mild to profound [4]. Although there is currently no specific medication for treating ASD, early and accurate diagnosis and intervention are considered the most effective approach. However, existing diagnostic methods—such as questionnaires and behavioral observation—are subjective and influenced by environmental factors, increasing the risk of misdiagnosis. Therefore, there is an urgent need for more accurate diagnostic methods and the identification of additional biomarkers to aid in diagnosis.

With the rapid development of medical imaging technology, tools for analyzing neurophysiology have become increasingly important. Functional Magnetic Resonance Imaging (fMRI) is a non-invasive neuroimaging technique [5] that measures Blood Oxygen Level Dependent (BOLD) signal changes due to neuronal activity across the brain at various time points [6]. Many studies have demonstrated the feasibility of using resting-state fMRI (rs-fMRI) to explore brain network interactions in patients with psychiatric disorders. In recent years, numerous researchers have combined deep learning techniques with rs-fMRI to explore psychiatric disorders, achieving significant results [7], [8]. Most studies use pre-defined brain templates to divide the brain into regions of interest (ROIs), obtain the BOLD time series of these ROIs, and then compute the correlations between the time series to construct functional connectivity networks (FCNs), enabling brain activity analysis [9], [10].

In ASD diagnosis using rs-fMRI data, researchers often integrate datasets from multiple medical centers to address the scarcity of training data [11]. However, due to the heterogeneity in equipment, scanning parameters, and data characteristics across different medical centers, there are significant differences in the data distributions between centers, leading to the domain shift problem [12]. This discrepancy severely limits the generalization ability of models, especially when diagnostic labels are absent for data from certain medical centers, making traditional supervised learning methods difficult to apply directly. To address this issue, Domain Adaptation (DA) [13] techniques have emerged. The goal of DA is to enable knowledge transfer from the source domain to the target domain through techniques like feature alignment, thereby

improving classification performance in the target domain. This approach provides a novel perspective for ASD diagnosis based on multi-site data. Currently, depending on the number of source domains, DA methods can be categorized into Single-Source Domain Adaptation (SSDA) [14] and Multi-Source Domain Adaptation (MSDA) [15].

Single-source domain adaptation, as the name suggests, involves a source domain dataset with labeled data from a single site and a target domain dataset from an unlabeled site. The goal is to reduce the feature distribution difference between the source and target domains, allowing the model to perform well in classifying data from the target domain. Chu et al. [16] proposed an adaptive framework for multi-site rs-fMRI, based on Attention Graph Convolutional Networks (A²GCN), for brain disease identification. This approach uses graph convolutional networks to extract features from functional connectivity networks and employs an attention mechanism to capture the importance of different brain regions. Additionally, it minimizes the data distribution discrepancy between the source and target domains by constraining the mean absolute error (MAE) and CORAL [17] of sample features, thereby improving the model's generalization and interpretability. Experimental results show that this method achieves promising results in single-source domain adaptation for ASD classification tasks and helps explore shallow pathological brain regions. Fang et al. [18] proposed an unsupervised cross-domain fMRI adaptation framework based on discrepancy for the automated identification of Major Depressive Disorder. The method first extracts spatiotemporal features from both source and target domain data through an attention-guided graph convolution module. Then, a module based on the Maximum Mean Discrepancy (MMD) [19] constraint is designed to align features between labeled source domain data and unlabeled target domain data. Experiments with rs-fMRI data from 681 subjects demonstrate the superior performance of this method, which also helps localize disease-related functional connectivity abnormalities, providing support for clinical analysis of psychiatric disorders using fMRI.

Single-source domain adaptation methods have achieved some success in brain disease diagnosis using multi-site data. By aligning and transferring features between a labeled source domain and an unlabeled target domain, these methods enhance the model's generalization ability in the target domain. However, these methods have clear limitations. Specifically, single-source methods are only applicable to simple cross-domain adaptation scenarios between a source and target domain. In real-world problems, there are typically multiple source domains with labeled data, each from different sources but potentially exhibiting significant differences in data characteristics (i.e., multi-source domains). Single-source methods fail to fully utilize the information from multiple source domains, which can lead to a decline in model performance in more complex cross-domain scenarios. Therefore, researching multi-source domain adaptation methods is crucial to better address the challenges posed by multi-site data analysis in practical settings.

Traditional single-source domain adaptation methods struggle to fully utilize the rich information from multiple source

domains, making them inadequate for addressing the heterogeneity and distribution discrepancies inherent in multi-site data. To overcome these limitations, multi-source domain adaptation methods have emerged. These methods aim to integrate knowledge from multiple source domains and improve the model's adaptation to unlabeled data from the target domain through effective feature alignment strategies. This enables better handling of cross-domain brain disease diagnosis challenges. For instance, Li et al. [20] proposed a privacy-preserving federated learning framework combined with domain adaptation techniques for multi-site fMRI data analysis, specifically for ASD diagnosis. This method trains models locally at each site and aggregates updates into a global model, thus protecting patient privacy. It also incorporates domain adversarial techniques [21] and expert mixture strategies [22] to reduce the distribution differences across sites, providing a new perspective for ASD diagnosis with multi-source data.

Furthermore, other approaches, such as BrainDAS by Song et al. [11] and LRCDR by Liu et al. [23], demonstrate the effectiveness of multi-source domain adaptation in improving classification accuracy and generalization ability in multi-site brain disease diagnosis. BrainDAS utilizes a structure-aware domain adaptation network to address domain shift by modeling both local and global brain network structures, reducing feature discrepancies across sites through joint feature learning and domain adversarial training. Meanwhile, LRCDR employs low-rank and class-discriminative representations to enhance the model's robustness and categorization ability by capturing global structural information and minimizing distribution gaps between source and target domains. Compared to traditional methods, these multi-source domain adaptation approaches show stronger generalization and higher classification performance in tasks like ASD recognition, making them more suitable for addressing multi-site fMRI data analysis challenges.

Deep learning algorithms based on domain adaptation have demonstrated significant potential in the analysis of multi-site fMRI data. These methods effectively address issues such as discrepancies in data distribution across sites and the absence of labeled data in the target domain, thereby greatly enhancing model adaptability and classification performance in the target domain. Single-source domain methods laid the foundation for this field but are limited in scope as they can only handle simple scenarios involving a single source and a single target domain. In contrast, multi-source domain methods integrate data from multiple source domains, enabling more comprehensive feature alignment and stronger model generalization.

Innovative approaches such as domain adversarial techniques, low-rank representation, and class-discriminative strategies have expanded the applicability of domain adaptation methods and provided more objective, efficient, and reliable tools for clinical ASD diagnosis. However, current methods still fall short in several aspects, including suboptimal performance, inconsistent experimental protocols, and insufficient model interpretability and exploration of pathological mechanisms.

To address these challenges, we propose a domain adap-

tation algorithm based on hyperbolic space embedding. The hyperbolic space naturally captures the topological structure of brain functional networks. We leverage this property to embed brain functional networks into hyperbolic space, constructing community networks in the hyperbolic domain for effective brain representation. To tackle the heterogeneity of multi-site data, we introduce Hyperbolic Maximum Mean Discrepancy for marginal distribution alignment (global alignment) between source and target domains. For conditional distribution alignment, we align the class prototypes derived from source domain labels with those generated from pseudo-labels in the target domain, ensuring more precise feature alignment.

Our main contributions are summarized as follows:

(1) We propose a novel approach that leverages the geometric properties of hyperbolic space to represent brain functional networks, effectively capturing the complex topological structures of these networks.

(2) To address the marginal distribution differences in multi-site data, we design an innovative Hyperbolic Maximum Mean Discrepancy method, significantly reducing global distribution discrepancies between source and target domains.

(3) We introduce a category prototype alignment strategy, which aligns source domain category prototypes with pseudo-label prototypes from the target domain. This approach achieves conditional distribution alignment between domains, further enhancing classification performance.

(4) By integrating marginal and conditional distribution alignment strategies, we construct a unified domain adaptation framework. This framework effectively addresses the heterogeneity of multi-site data and category shifts, improving the generalization ability of the model.

(5) Extensive experiments validate the effectiveness of our proposed method.

II. PRELIMINARIES

A. Hyperbolic Embedding and Hyperbolic Graph Convolutional Networks

In this section, we introduce hyperbolic embeddings (with a focus on the Poincaré disk) and their application in Graph Convolutional Networks (GCNs). This discussion aims to provide a deeper understanding of how the unique properties of hyperbolic geometry can be leveraged to represent and learn complex network structures more effectively.

1) *Hyperbolic Embedding*: In many real-world complex networks, such as social networks, communication networks, and biological networks, relationships between nodes often exhibit strong hierarchical structures or non-Euclidean geometric characteristics [24]–[26]. Traditional Euclidean embedding methods face limitations in modeling these structures, as their ability to represent large-scale data diminishes rapidly with increasing dimensions, a phenomenon known as the “curse of dimensionality”. In contrast, hyperbolic geometry offers a more efficient approach to spatial representation. It is inherently well-suited for capturing hierarchical and tree-like data structures [27], as distances in hyperbolic space grow exponentially, enabling a more compact representation of complex relationships between nodes. Among the various

models of hyperbolic space, the Poincaré disk model [28] is one of the most commonly used representations.

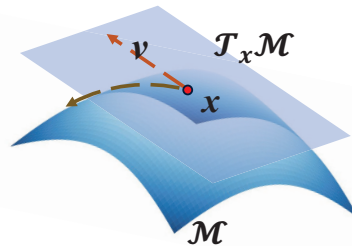


Fig. 1. The tangent space $T_x M$ is a vector space associated with a specific point x on a curve that lies within the manifold M . A tangent vector v at x resides in the tangent space $T_x M$ and represents the direction of the curve as it passes through x .

The Poincaré disk model defines a hyperbolic space with constant negative curvature, where the set of points is confined within a unit disk [26]. For the unit disk: $D_c = \{x \in R^n : \|x\|_2 < \frac{1}{\sqrt{c}}\}$ (where c is the curvature and $\|\cdot\|_2$ denotes the standard euclidean inner product) the metric defines the distance between any two points u and v as (1):

$$d(u, v) = \frac{2}{\sqrt{c}} ar \tanh(\sqrt{c} \| -u \oplus v \|_2) \quad (1)$$

where \oplus stands for the Möbius addition:

$$u \oplus v = \frac{\left(1 + 2c \langle u, v \rangle + c \|v\|_2^2\right) u + \left(1 - c \|u\|_2^2\right) v}{1 + 2c \langle u, v \rangle + c^2 \|u\|_2^2 \|v\|_2^2} \quad (2)$$

For feature vectors or time series in Euclidean space, embedding in the Poincaré disk can be achieved through the corresponding mapping function (3). Conversely, embedding from the Poincaré disk to Euclidean space can be accomplished through the mapping function (4). The embeddings from Euclidean space to hyperbolic space and vice versa are illustrated in Figure 1.

$$\exp_0^c(x) = \tanh(\sqrt{c} \|x\|_2) \frac{x}{\sqrt{c} \|x\|} \quad (3)$$

$$\log_0^c(x) = \frac{1}{\sqrt{c}} ar \tanh(\sqrt{c} \|x\|_2) \frac{x}{\|x\|_2} \quad (4)$$

2) *Hyperbolic Graph Convolutional Networks*: Graph Convolutional Networks are powerful deep learning methods for handling graph data. However, traditional GCNs are typically based on Euclidean space, which fails to fully leverage the hierarchical structure and complex relationships inherent in graph data. Extending GCNs to hyperbolic space allows for more efficient capture of the hierarchical relationships within the graph [29].

In the process of transforming features in hyperbolic space, the traditional matrix multiplication used in Euclidean space is no longer applicable. Instead, the feature transformation in hyperbolic space is defined as follows:

$$x^l = Proj(W^l \otimes x^{l-1} \oplus b^l) \quad (5)$$

TABLE I
DEMOGRAPHIC INFORMATION OF THE FOUR SITES INVOLVED IN THIS STUDY

Site	ASD		CN		Scanner
	Age (Mean±std)	Gender (M/F)	Age (Mean±std)	Gender (M/F)	
NYU	14.92±7.04	64/9	15.67±6.19	72/26	SIEMENS Allegra
UM	13.85±2.29	39/9	15.03±3.64	49/16	GE Signa
USM	24.60±8.46	38/0	22.33±7.70	23/0	SIEMENS Trio
UCLA	13.34±2.56	34/2	13.18±1.76	33/6	SIEMENS Trio

where $Proj$ denotes the projection operation, which ensures that the result remains within the Poincaré disk. The symbol \otimes represents the Möbius Scalar Multiplication as (6).

$$W \otimes x = \tanh \left(\frac{\|xW^T\|_2}{\|x\|_2} \operatorname{ar} \tanh(\sqrt{c}\|x\|_2) \right) \frac{xW^T}{\sqrt{c}\|xW^T\|_2} \quad (6)$$

For a graph $G(V, A)$ (V represents the node features and A represents the adjacency matrix of the graph), a single layer of graph convolution on the hyperbolic manifold can be represented as:

$$H = \exp_0^c(\sigma(A(\log_0^c(HLinear(V, W)))))) \quad (7)$$

Here, we use $HLinear$ to represent the feature transformation process (as (5)) in hyperbolic space, where σ denotes the corresponding activation function.

B. Brain Functional Gradients

The brain's functional gradients, by capturing the continuous spatial patterns of extrinsic connectivity between isolated networks, offers a more comprehensive perspective of brain organization [30], [31]. A gradient-based approach, a nonlinear decomposition of high-dimensional resting-state functional connectivity, can identify the functional hierarchy of the brain by representing its connections in a continuous low-dimensional space [7]. Functional gradients have been widely applied in brain analysis, and in the context of various psychiatric disorders, they can reveal abnormal functional hierarchies across brain regions [7], [32], [33].

Functional gradients have also been used in the study of Autism Spectrum Disorder. For instance, Hong et al. [34] identified functional gradient disruptions in individuals with autism, indicating a reduction in functional independence between regions, particularly between unimodal and transmodal regions. Urchs et al. [35] further explored functional gradient analysis in ASD using the ABIDE-I dataset [36], revealing gradient compression, which suggests reduced functional segregation in ASD patients.

Building on our previous research [37], we apply functional gradients in the same manner to partition brain community networks. This approach leverages the functional relationships between ROIs to construct corresponding functional community networks.

In previous methods for calculating functional gradients, BrainSpace [38] was typically used for direct computation. However, since the functional connectivity network in this

study is embedded in hyperbolic space, while traditional methods are primarily designed for Euclidean space, adjustments were necessary in our approach. Specifically, for the computation of the affinity matrix, we utilized the Spearman correlation coefficient (as shown in (8)), rather than the cosine similarity, which is commonly used in Euclidean space but is not suitable for hyperbolic geometry. This modification allows us to more accurately capture the non-Euclidean relationships between brain regions within hyperbolic space.

$$Aff_{spearman}(i, j) = \frac{\operatorname{cov}(r_i, r_j)}{\sigma_{r_i}\sigma_{r_j}} \quad (8)$$

where r_i and r_j represent the rank vectors of variables i and j , respectively, cov denotes the covariance between the rank vectors, and σ_{r_i} and σ_{r_j} indicates the standard deviation of the rank vectors.

Before performing the nonlinear dimensionality reduction on the affinity matrix, we first apply sparsification to the matrix. Specifically, we retain only the top 10% [33], [38] of the strongest functional connections for each ROI, thereby extracting the most significant connections. Next, we normalize the sparse affinity matrix, where D denotes the degree matrix of the affinity matrix, and α represents the diffusion parameter, which is empirically set to a common value of 0.5 [38].

$$W(a) = D^{-\frac{1}{\alpha}} \cdot Aff_{spearman} \cdot D^{-\frac{1}{\alpha}} \quad (9)$$

Subsequently, we use diffusion mapping to extract the components of the functional gradient. This step implements the capture of nonlinear relationships within the data, where D_α represents the diagonal matrix, with $D_{\alpha i, i} = \sum_{j=1}^{N_R} W_{i, j}$.

$$P(\alpha) = D_\alpha^{-1} W(\alpha) \quad (10)$$

Next, we perform eigenvalue decomposition to extract the top n largest eigenvalues λ and their corresponding eigenvectors v .

$$P(\alpha)v = \lambda v \quad (11)$$

Finally, the diffusion embedding is constructed by scaling the eigenvectors to obtain the i -th functional gradient component Φ_i .

$$\Phi_i = \frac{\lambda_i}{1 - \lambda_i} \cdot v_i \quad (12)$$

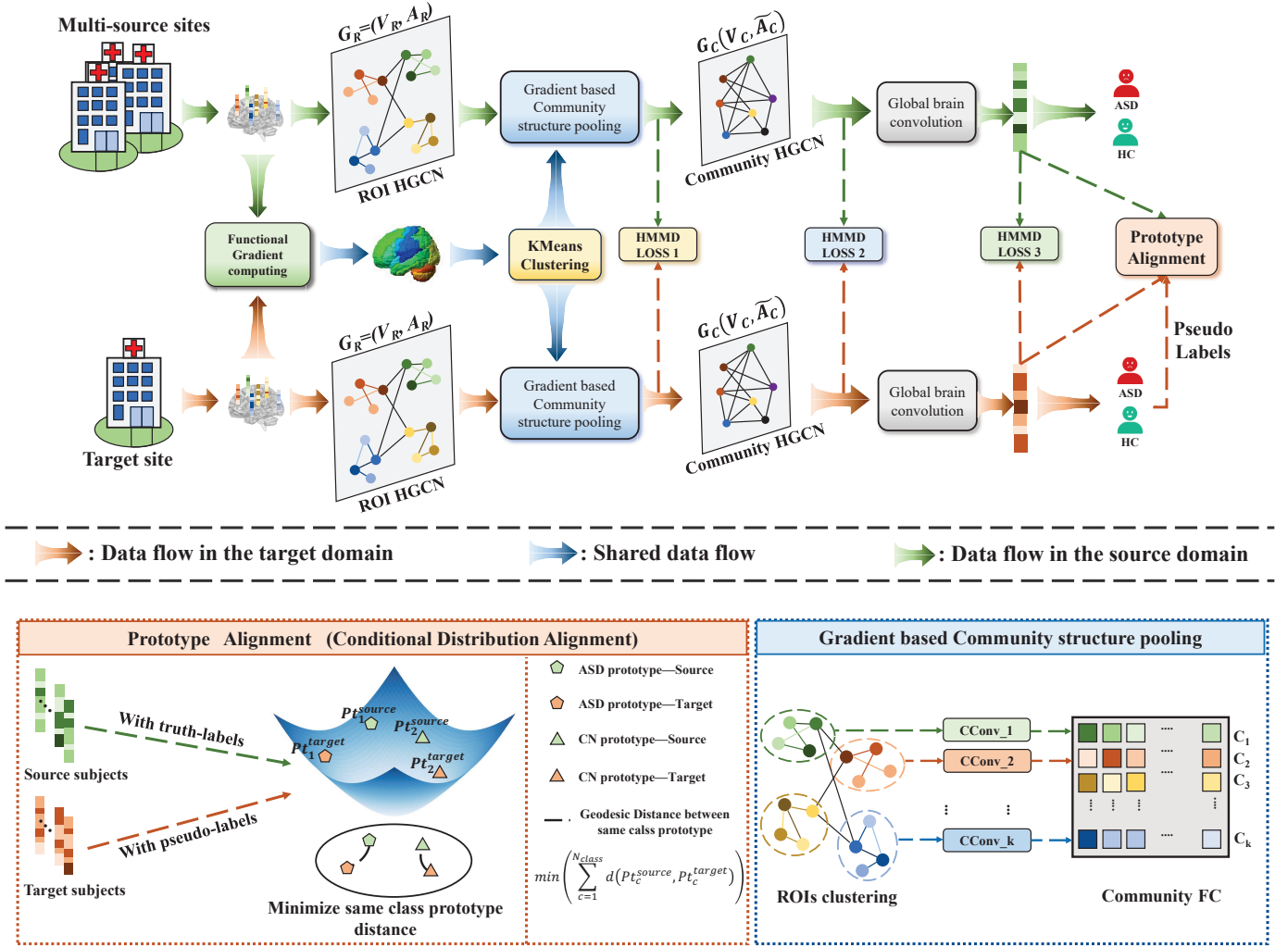


Fig. 2. The diagram of the proposed Hyperbolic Hierarchical Multi-Sites Domain Alignment (H²MSDA) method for ASD identification.

III. MATERIALS AND PROPOSED METHOD

A. Materials and data preprocessing

In this study, the domain adaptation experiments were conducted using data from the four largest sites in the ABIDE (Autism Brain Imaging Data Exchange) dataset [36]: NYU, UM, UCLA, and USM. These sites were selected based on their substantial sample sizes, which provide rich data support for the domain adaptation tasks. Additionally, the significant heterogeneity of the data across different sites creates an ideal experimental environment to validate the effectiveness of the domain adaptation methods. The statistical information for the data selected from each site is shown in Table I.

We used the resting-state fMRI data processing toolbox (DPARSF) for standardization and preprocessing of the rs-fMRI data [39]. The specific preprocessing steps are as follows: 1. Discard the first 5 time points to ensure signal stability. 2. Perform slice timing correction to correct for the acquisition delays between slices. 3. Apply motion correction to reduce the influence of head movement on the signals. 4.

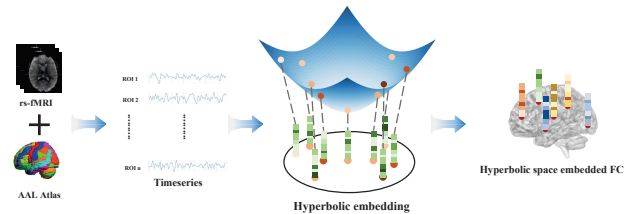


Fig. 3. The pipelines process and computation of functional connectivity network.

Normalize the images to the MNI space using the EPI template and resample them to a $3 \times 3 \times 3$ mm resolution. 5. Apply spatial smoothing using a Gaussian kernel with a full-width at half-maximum (FWHM) of 4 mm. 6. Perform linear detrending and apply band-pass filtering (0.01–0.10 Hz) to extract the relevant BOLD signals. 7. Remove nuisance signals, including head motion parameters, white matter signals, cerebrospinal fluid (CSF) signals, and global signals.

After completing the above preprocessing steps, the normalized fMRI data were partitioned into 116 ROIs using the AAL template [40], and the BOLD time series of each ROI were extracted. To avoid amplitude differences between different ROIs affecting subsequent analysis, the BOLD time series of each ROI were standardized, enhancing the model's robustness and the effectiveness of feature extraction.

B. Proposed Method

In this experiment, we leverage the efficient representation capability of hyperbolic space to embed brain functional networks within it. By embedding the functional networks into this space, we can achieve precise representation and, using domain adaptation techniques, enable effective transfer between the source and target domains to perform unsupervised diagnostic tasks on the target domain. Additionally, this method significantly alleviates the data heterogeneity problem across different sites, improving the model's generalization ability and diagnostic accuracy. The proposed method is shown in Figure 2.

Specifically, for the feature extraction of brain functional networks, we use hyperbolic space-based Graph Convolutional Networks (HGNC) to enable effective message passing at the ROIs level. Then, we apply functional gradients (which are derived from the hyperbolic embedding and computed in hyperbolic space) to explore and construct community networks. Through the construction of these community networks, we obtain community-level functional networks. Similarly, we employ HGNC to facilitate message passing between the communities, which better simulates the brain's true structure. Finally, through whole-brain scale convolutions, we extract vector-level representations of the entire brain network, enabling the final diagnostic classification.

1) Hyperbolic Embedding and ROI-Level Feature Extraction:

After preprocessing, we obtain the BOLD time series for each ROI. To effectively construct the hyperbolic embedded functional network, we first embed the BOLD time series of each brain region into the Poincaré disk.

For the BOLD time series embedded into the Poincaré disk, to build an effective functional network, as in [41], we select the Spearman correlation coefficient (13) to compute the pairwise correlation between the time series of brain regions. This choice is made instead of using the Pearson correlation coefficient, which is typically used for calculating functional connectivity in Euclidean space. Pearson correlation measures linear relationships, which are not suitable for manifold spaces. In contrast, the Spearman correlation can capture non-linear relationships, making it more appropriate for our manifold-based approach.

$$\rho = \frac{\text{cov}(rx, ry)}{\sigma_{rx}\sigma_{ry}} \quad (13)$$

Where rx and ry represent the rank vectors of variables x and y , respectively, cov denotes the covariance between the rank vectors, and σ_{rx} and σ_{ry} indicates the standard deviation of the rank vectors.

Through the steps outlined above, we obtained the FC embedded in the Poincaré disk for each subject. To enable effective message passing between the ROIs, we employed the Hyperbolic Graph Convolutional Network on the hyperbolic space.

Considering the presence of many noisy connections in the functional connectivity network, following [42], we empirically retain the top 10% of the strongest connections as the adjacency matrix A_R . The hyperbolic embedded FC serves as the node features V_R in the graph network. This results in a corresponding ROI-level graph $G_R(V_R, A_R)$. To enable message passing between the ROIs, we apply a single layer of Hyperbolic Graph Convolutional Network, as shown in the following (14):

$$H_R = \exp_0^c(\sigma(A_R(\log_0^c(HLinear(V_R, W_R)))))) \quad (14)$$

Functional connectivity during resting state exhibits a significant modular structure, which facilitates efficient information communication and cognitive functions [43], [44]. Community networks play a critical role in understanding the functional organization of the brain [45]. Functional communities have been shown to be closely related to cognitive behaviors [46], mental states [47], and neuropsychiatric disorders [48]. Moreover, recent studies have confirmed that the brain's modularity can serve as a unified biomarker for intervention-related plasticity [49], [50].

Generally, each community is composed of tightly connected brain ROIs, which are sparsely connected to ROIs in other communities [44]. The functional similarity between these ROIs can be effectively captured using the functional gradient. Similar to our previous work [37], we input the group-level average FC into BrainSpace to obtain functional gradients for multiple components. The gradients of the top N_{gra} components are then used for KMeans clustering, enabling the assignment of the 116 ROIs to k communities.

To achieve effective feature representation of the community network, we propose the $CConv$ module, which is specific to each community. Specifically, we use a conv1d to extract features from the ROIs that belong to the same community, thereby achieving the feature representation of the community, as expressed by the following formula (15).

$$C_i = \sigma(LN(\text{conv1D}_i(ROIs_i))) \quad (15)$$

where $ROIs_i$ represents the feature matrix of the ROIs belonging to the i -th community, LN denotes layer normalization, and σ is the activation function. It is important to note that since conv1D can only be implemented in Euclidean space, the features of the ROIs used in this process are first transformed from hyperbolic space to Euclidean space using the transformation defined in (4).

2) Community-level HGNC and Whole-Brain Representation

Extraction: To closely simulate the message-passing dynamics between functional brain communities, we propose a community-level functional network implemented through Hyperbolic Graph Convolutional Networks, which effectively enables information exchange across communities and facilitates

the exploration of their complex interrelationships. For the definition of the intricate connection structure within the community network, we refer to the approach proposed in [51], where the interaction between each community and the others is modeled using the dot product of their respective features, thereby capturing the functional relationships between communities. This connection model is both dynamic and instance-specific. We assume that global connections are undirected, as the relationship between two local graphs is inherently reciprocal. Therefore, the adjacency matrix $A_C \in R^{k \times k}$ of the community graph is defined as follows:

$$A_{C-base} = \begin{pmatrix} C_1 \cdot C_1 & \cdots & C_1 \cdot C_k \\ \vdots & \ddots & \vdots \\ C_1 \cdot C_k & \cdots & C_k \cdot C_k \end{pmatrix} \quad (16)$$

Here, \cdot stands for the dot product.

To better capture and learn the complex relationships between functional communities, this study employs a symmetric, trainable attention matrix to emphasize the important connections in the similarity adjacency matrix. It is important to note that the attention matrix is also symmetric, as the adjacency matrix is undirected. The attention matrix M_C is defined as follows:

$$M_C = \begin{pmatrix} w_{1,1} & \cdots & w_{1,k} \\ \vdots & \ddots & \vdots \\ w_{k,1} & \cdots & w_{k,k} \end{pmatrix} \quad (17)$$

Therefore, the complete construction of the functional community network adjacency matrix is given by the following (18):

$$A_C = \sigma_{relu}(A_{C-base} \circ M_C) + I \quad (18)$$

Where \circ represents the Hadamard product, and I denotes the identity matrix. The inclusion of the identity matrix ensures that the adjacency matrix has self-connections. By adding the identity matrix after the activation function, we can emphasize the strength of self-connections.

Here, it is important to note that the obtained community adjacency matrix A_C differs from the ROI adjacency matrix A_R . A_R has already been normalized and then sparsified within the range of -1.0-1.0. However, A_C has not undergone normalization. Therefore, before inputting the community adjacency matrix A_C into the community HGNCN, normalization is required. The normalized community adjacency matrix can be computed using the following formula:

$$\tilde{A}_C = \tilde{D}^{-\frac{1}{2}} A_C \tilde{D}^{-\frac{1}{2}} \quad (19)$$

Where \tilde{D} denotes the degree matrix of A_C .

At this point, the corresponding functional community network graph $G_C(V_C, \tilde{A}_C)$ can be constructed and input into a single layer of HGNCN for message passing and feature transformation between the community networks.

$$H_C = \exp_0^c \left(\sigma \left(\tilde{A}_C (\log_0^c (HLinear(V_C, W_C))) \right) \right) \quad (20)$$

To further compress and represent the features, we designed a whole-brain-scale convolutional layer to achieve a comprehensive representation of the entire brain. This Conv2D uses kernels with the same size as the community networks to capture global brain relationships. To learn the whole-brain relationships from multiple perspectives, we employed multiple kernels (32 kernels in total). For effective Conv2D, the features are first mapped to Euclidean space using the logarithmic map as shown in (4) before applying the convolution.

Following the whole-brain-scale convolution, we obtain the feature vector representation for each subject. A single *HLinear* layer is subsequently employed to perform the final classification. To optimize the model parameters, the cross-entropy loss function (21) is utilized to guide the training process and minimize the classification error.

$$L_{CE} = \frac{1}{N} \sum_i^N - [y_i \times \log(p_i) + (1 - y_i) \times \log(1 - p_i)] \quad (21)$$

3) Hyperbolic Space Domain Alignment and Prototype Learning: For diagnostic classification across multiple sites, especially when the target site data lacks labeled annotations, directly applying a model trained on the source domain to predict target domain data often leads to suboptimal performance due to domain shift and data heterogeneity between the sites.

Maximum Mean Discrepancy is a non-parametric method used to measure the discrepancy between two distributions P and Q . The core idea of MMD is to compare the distances between the means of these distributions after mapping them into a Reproducing Kernel Hilbert Space defined by a Gaussian kernel [52]. In the context of hyperbolic space (Poincaré disk model), both the data distribution and the distance metric differ from Euclidean space. Therefore, MMD needs to be redefined to align with the characteristics of hyperbolic geometry. We propose the Hyperbolic MMD (HMMD), which is based on the hyperbolic distance metric, and the Gaussian kernel in hyperbolic space is defined as follows:

$$K_G(u, v) = \exp\left(-\frac{d(u, v)}{\gamma}\right) \quad (22)$$

To further enhance the expressiveness of the kernel, we employ a multi-bandwidth Gaussian kernel, defined as:

$$K_G(u, v) = \sum_{i=1}^L \exp\left(-\frac{d(u, v)}{\gamma_i}\right) \quad (23)$$

where L represents the number of Gaussian kernels, and γ_i denotes the bandwidth for each kernel.

Given a source domain sample $\{x_i\}_{i=1}^n \sim S$ and a target domain sample $\{y_j\}_{j=1}^m \sim T$, the HMMD can be represented as:

$$HMMD(S, T) = E_{x, x' \sim S} [K_G(x, x')] + E_{y, y' \sim T} [K_G(y, y')] - 2E_{x \sim S, y \sim T} [K_G(x, y)] \quad (24)$$

To achieve better alignment, as shown in Figure 2, we perform HMMD alignment on the features before and after

the community graph network, as well as on the final representation vectors for feature alignment.

The proposed HMMD alignment achieves marginal distribution alignment, for conditional distribution alignment, inspired by [53], we introduce prototype alignment to accomplish this task. Specifically, given all points $X_c = \{x_1, x_2, x_3 \dots, x_{N_c}\}$ of a particular class c , where N_c denotes the total number of samples in class c , the first point is selected as the base point x_{base} . The relative displacement of each point with respect to the base point is then computed. The average of all such relative displacements is subsequently calculated. Finally, the averaged relative displacement is mapped back to x_{base} , resulting in the class prototype, as shown in (25).

$$Pt_c = x_{base} \oplus \frac{1}{N_c} \sum_{i=1}^{N_c} (-x_{base} \oplus x_i) \quad (25)$$

Since the target domain lacks labeled data, we utilize the predicted labels (pseudo-labels) from the alignment step as surrogate ground truth labels to compute the corresponding prototypes. Finally, the hyperbolic distance between the prototypes of the same class in both domains is calculated using (26), leading to the Prototype Alignment (PA) Loss.

$$L_{PA} = \sum_{c=1}^{N_{class}} d(Pt_c^{source}, Pt_c^{target}) \quad (26)$$

Therefore, our final objective function can be expressed as L_{total} :

$$L_{total} = L_{CE} + \lambda_m (HMMD_1 + HMMD_2 + HMMD_3) + \lambda_{PA} L_{PA} \quad (27)$$

where L_{CE} represents the cross-entropy loss, $HMMD_i$ refers to the marginal distribution alignment loss at different layers, and L_{PA} denotes the conditional distribution alignment loss (Prototype Alignment Loss). λ_m and λ_{PA} are the weight hyperparameters associated with $HMMD_i$ and L_{PA} , respectively.

During the testing phase, we obtain the representation vectors from the test data and compute the distance between the test vectors and the source domain class prototypes to predict the class of the test data. Here, we do not incorporate the prototypes generated from the target domain data, as the pseudo-labels of the target domain are relatively unstable and may introduce instability during the testing phase.

IV. EXPERIMENTAL DESIGN AND RESULTS ANALYSIS

A. Experimental Setup

We adopted a 5-fold cross-validation strategy for the experiments, utilizing data from four sites: NYU, UM, USM, and UCLA. Two experimental validation strategies were employed: Experiment Validation Strategy 1: Each site is used sequentially as the target domain. The data from the current target domain is split into 5 folds, with one fold used as the test set and the remaining four folds as the training data (without real labels) for domain alignment. The data from

the other three sites (with real labels) serve as the source domain for training. Experiment Validation Strategy 2: This strategy aimed to assess the reliability of the baseline model by evaluating its performance without domain alignment. Specifically, all site data were combined and randomly shuffled, and classification was performed directly on the mixed data without any domain adaptation. A 5-fold cross-validation was then conducted on the merged dataset. These two experimental validation strategies are illustrated in Figure 4.

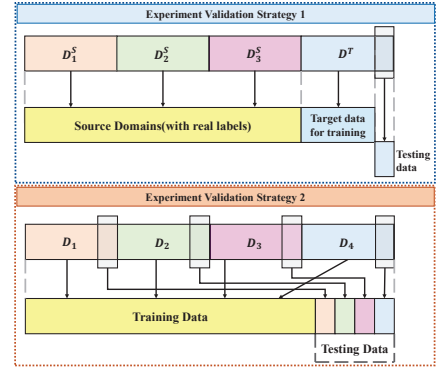


Fig. 4. The difference between two experimental validation strategies.

For the classification performance of the model, we utilized four metrics, which include accuracy, specificity, sensitivity, and F1 score. The corresponding formulas for these metrics are as follows:

$$Acc = \frac{TP + TN}{TP + FN + FP + TN} \quad (28)$$

$$Sen = \frac{TP}{TP + FN} \quad (29)$$

$$Spe = \frac{TN}{TN + FP} \quad (30)$$

$$F1 = \frac{2TP}{2TP + FP + FN} \quad (31)$$

B. Compared Methods

In the experiment, we compared our H²MSDA method with the following approaches, which include seven domain adaptation methods and four non-domain adaptation methods.

Compared domain adaptation methods:

1) **A²GCN** [16]: This method focuses on utilizing a Graph Convolutional Network enhanced with attention mechanisms for domain adaptation in the analysis of resting-state fMRI data, specifically for brain disorder identification. The approach aims to address the challenge of domain shift between different fMRI datasets (source and target domains) by effectively transferring knowledge from a source domain with labeled data to a target domain with no labels. The method employs an attention-based mechanism to adaptively weigh the importance of different brain regions, allowing for more accurate identification of brain disorders.

2) **Fed_Align** [20]: Fed_Align is a federated learning-based domain adaptation method that aims to align data distributions across multiple fMRI sites for improved analysis and

diagnosis. It addresses the challenge of heterogeneous fMRI data from different sites by aligning the feature distributions between source and target domains. The method works by applying domain alignment techniques directly on the federated learning framework, ensuring that the models trained on each site’s data are aligned before they are aggregated.

3) **TMJDA** [54]: TMJDA introduces a novel transport-based framework for joint distribution alignment in multi-site fMRI data, specifically targeting improvements in the classification of Autism Spectrum Disorder. The method innovatively combines optimal transport theory with distribution alignment, enabling more precise modeling of brain functional connectivity across diverse datasets.

4) **maLRR** [55]: maLRR is a domain adaptation method designed to improve the identification of Autism Spectrum Disorder (ASD) from multi-site fMRI data by addressing the domain shift between different sites. The method leverages low-rank regression to capture shared information across sites while adapting the model to reduce site-specific biases. The key idea is to learn a common subspace that effectively aligns the features from different sites, thus improving the generalizability of ASD classification models in multi-site studies.

5) **Fed.MOE** [20]: Fed.MOE (Federated Mixture of Experts) is another federated learning-based method that introduces a mixture of experts (MOE) model for handling domain adaptation across multiple fMRI sites. The method adapts a mixture of experts model to federated learning, where different experts are specialized to learn features from different domains (i.e., sites). The global model learns to assign data from each site to the most relevant expert, improving both domain adaptation and model performance.

6) **TP-MIDA** [56]: TP-MIDA is a shallow domain adaptation method designed for multi-site autism classification. The method utilizes Tangent Person Embedding to construct higher-order brain functional connectivity. It then applies a maximum independence domain adaptation approach by maximizing the data variance while minimizing the statistical dependence on the site, thereby reducing site heterogeneity. The goal of TP-MIDA is to improve the classification performance by effectively addressing the variation across different sites while preserving the relevant features for autism diagnosis.

7) **LRCDR** [23]: LRCDR is a domain adaptation method designed for Autism Spectrum Disorder identification, addressing the distributional differences across fMRI data from multiple sites. The method integrates low-rank representations with class discriminative features to reduce heterogeneity between sites and improve multi-site ASD classification performance.

Compared non-domain adaptation methods:

1) **f-GCN** [57]: F-GCN is a basic graph convolutional network. The focus of this method is to choose the appropriate threshold to remove redundant connections, with the optimal threshold identified in our experiment being 0.3. In f-GCN, multiple GCN layers are stacked. The model employs a global average pooling operator to generate a coarse graph, which reduces the number of parameters by decreasing the size of the representation and thus helps avoid overfitting. The readout

layer then consolidates the node representations into a single graph representation.

2) **BrainNetCNN** [58]: BrainNetCNN is a convolutional neural network designed specifically for brain network analysis. By incorporating Edge-to-Edge, Edge-to-Node, and Node-to-Graph layers, it effectively extracts hierarchical features that capture the complex interactions within brain networks. This method enhances the model’s ability to predict neurodevelopmental outcomes, making it a powerful tool for studying brain development and disorders.

3) **MVS-GCN** [59]: MVS-GCN is a multi-view graph convolutional network guided by prior brain structure learning. It integrates functional and structural connectivity to capture complementary brain network information while leveraging prior knowledge for biologically meaningful feature learning. The model’s innovative fusion strategy and graph-based architecture lead to improved ASD diagnosis, providing a robust tool for brain disorder classification.

4) **MCG-Net** [60]: MCG-Net is a dual-branch network architecture. This method employs parallel convolution and graph convolution to respectively extract high-order representations and low-order spatial features of functional connectivity networks. Ultimately, the extracted multi-features are fused and utilized in a downstream classification task through linear layers.

5) **ASD-HNet** [37]: ASD-HNet is a hybrid neural network model designed to hierarchically extract features from functional brain networks for Autism Spectrum Disorder identification. The main innovation of this approach lies in the use of functional gradients to construct functional communities, and in performing hierarchical feature extraction from a functional perspective. This enables the creation of an effective and interpretable auxiliary diagnostic model.

C. Result on Multi-Site data

In this section, we conducted experimental comparisons with other methods. The experimental results for the two different experiment validation strategies will be presented and analyzed as follows.

1) *Experiment Validation Strategy 1 Results*: Each site was sequentially selected as the target domain, while the remaining three sites served as the source domain. It is important to note that since the comparison includes non-domain adaptation methods, we employed 5-fold cross-validation on the data from each site for non-domain adaptation methods to ensure a fair comparison. In simpler terms, the unlabeled target domain data used for training in domain adaptation methods was instead used with labels for training in non-domain adaptation methods. The experimental results across the four sites are presented in Tables II and III.

From the experimental results, it is evident that the proposed method achieves superior performance in terms of accuracy across all four sites. Compared to the baseline methods, our approach demonstrates improvements of +4.02%, +2.65%, +4.74%, and +6.73% for NYU, UM, USM, and UCLA, respectively. While our method may not outperform others on every metric, it achieves a balanced performance in terms of

TABLE II

PERFORMANCE OF OUR PROPOSED MODEL COMPARED WITH STATE-OF-THE-ART METHODS ON NYU AND UM TARGET SITES. THE BEST RESULTS ARE PRESENTED IN BOLD. '*' INDICATES THAT THE RESULTS FOR THIS METHOD ARE DERIVED FROM THE ORIGINAL STUDY, WHILE '-' DENOTES THAT THE EXPERIMENTAL RESULTS ARE NOT REPORTED FOR THIS DATASET.

Group	Model	NYU				UM				Altas
		ACC	SEN	SPE	F1	ACC	SEN	SPE	F1	
Non-domain Adaptation	f-GCN	71.95	58.07	79.95	60.89	75.30	82.29	70.25	73.14	AAL
	BrainNetCNN	72.52	63.71	78.53	62.96	74.27	64.81	77.53	59.73	AAL
	MVS-GCN	74.87	74.87	53.01	71.78	70.87	70.87	52.14	64.44	AAL
	MCG-Net	71.98	54.22	83.05	59.59	78.77	70.86	81.73	68.94	AAL
	ASD-HNet	76.62	71.97	81.11	71.88	77.83	83.95	74.01	75.30	AAL
Domain Adaptation	A ² GCN	66.67	41.96	81.64	41.93	68.18	65.52	68.43	58.67	AAL
	Fed_Align	71.97	51.51	84.64	59.25	76.33	45.87	91.67	53.11	AAL
	TMJDA*	71.09	-	-	-	72.57	75.00	70.77	-	AAL
	maLRR*	71.88	66.67	78.57	-	72.73	76.92	66.67	-	AAL
	Fed_MOE	67.83	73.45	64.64	65.56	70.07	47.10	84.92	55.51	AAL
	TP-MIDA*	75.60	75.10	-	75.00	72.40	73.60	-	71.4	CC200
	LRCDR*	73.40	78.50	69.50	67.70	74.50	70.60	77.90	75.80	AAL
H ² MSDA(ours)	80.66	82.72	78.20	78.01	81.42	73.42	83.40	74.72	AAL	

TABLE III

PERFORMANCE OF OUR PROPOSED MODEL COMPARED WITH STATE-OF-THE-ART METHODS ON USM AND UCLA TARGET SITES. THE BEST RESULTS ARE PRESENTED IN BOLD. '*' INDICATES THAT THE RESULTS FOR THIS METHOD ARE DERIVED FROM THE ORIGINAL STUDY, WHILE '-' DENOTES THAT THE EXPERIMENTAL RESULTS ARE NOT REPORTED FOR THIS DATASET.

Group	Model	USM				UCLA				Altas
		ACC	SEN	SPE	F1	ACC	SEN	SPE	F1	
Non-domain Adaptation	f-GCN	80.12	70.62	86.66	79.61	80.00	59.21	89.14	64.71	AAL
	BrainNetCNN	78.59	83.42	69.62	81.71	70.67	47.36	86.43	52.39	AAL
	MVS-GCN	78.59	78.59	77.20	76.33	69.33	69.33	44.86	62.54	AAL
	MCG-Net	78.59	80.75	79.76	82.01	70.67	47.57	84.50	52.41	AAL
	ASD-HNet	83.72	88.61	76.48	87.29	69.33	64.36	75.16	65.26	AAL
Domain Adaptation	A ² GCN	73.72	74.26	65.29	75.98	69.33	57.50	73.86	59.11	AAL
	Fed_Align	67.44	61.33	79.17	69.47	72.00	51.79	90.83	61.14	AAL
	TMJDA*	80.18	-	-	-	73.10	-	-	-	AAL
	maLRR*	74.62	86.11	68.10	-	75.00	64.29	85.71	-	AAL
	Fed_MOE	73.72	97.50	32.50	80.30	65.33	82.44	45.01	67.27	AAL
	TP-MIDA*	79.30	80.70	-	77.80	82.60	82.80	-	81.70	CC200
	LRCDR*	74.30	75.90	72.10	75.20	71.70	70.40	73.30	74.60	AAL
H ² MSDA(ours)	88.46	94.17	76.00	91.11	89.33	71.03	91.11	72.76	AAL	

specificity and sensitivity, avoiding extreme distributions (e.g., very low sensitivity paired with very high specificity). This highlights the robustness and reliability of our approach, ensuring a more consistent performance across different metrics.

To visualize the data distribution of brain networks before and after domain adaptation, we applied t-SNE [11] to map the original brain networks and the extracted representation networks into a two-dimensional space. As shown in Figure 5, each point in the t-SNE scatter plot represents a sample of a brain network. The visualization clearly demonstrates that, after applying the alignment operation, the data distribution across different sites becomes more consistent, with no apparent domain shift. This result validates the effectiveness of the proposed method in addressing cross-domain heterogeneity.

2) *Experiment Validation Strategy 2 Results*: This validation strategy aims to assess the reliability of our baseline model by evaluating its performance in the absence of domain align-

TABLE IV

EXPERIMENT VALIDATION STRATEGY 2 RESULTS. THE BEST RESULTS ARE PRESENTED IN BOLD.

Methods	ACC	SEN	SPE	F1
f-GCN	65.71	54.76	73.99	59.42
BrainNetCNN	67.62	57.45	76.46	61.96
MVS-GCN	64.56	64.56	52.49	63.14
MCG-GCN	68.34	66.29	69.20	65.88
ASD-HNet	71.17	67.19	74.71	68.14
H ² MSDA(ours)	72.85	65.35	78.98	68.31

ment. Specifically, we directly classify using mixed site data without any domain adaptation. The data from all four sites is combined and shuffled, followed by 5-fold cross-validation. The resulting experimental outcomes are presented in Table IV. From the results, our baseline model achieved the best performance across multiple metrics, including accuracy (ACC,

TABLE V
ABLATION EXPERIMENTS ON NYU SITE. '-' INDICATES THAT THE LOSS IS NOT USED. '✓' DENOTES THAT THE USE OF THE LOSS

HMMD Loss1	HMMD Loss2	HMMD Loss3	Prototype Align	ACC	SEN	SPE	F1
-	-	-	-	74.22	61.58	84.09	65.39
✓	✓	✓	-	78.94	72.12	83.58	73.96
-	-	-	✓	77.76	76.68	78.65	74.43
-	✓	✓	✓	80.07	78.38	80.31	76.34
✓	-	✓	✓	80.07	81.05	78.20	76.93
✓	✓	-	✓	78.53	70.90	82.12	72.25
✓	✓	✓	✓	80.66	82.72	78.20	78.01

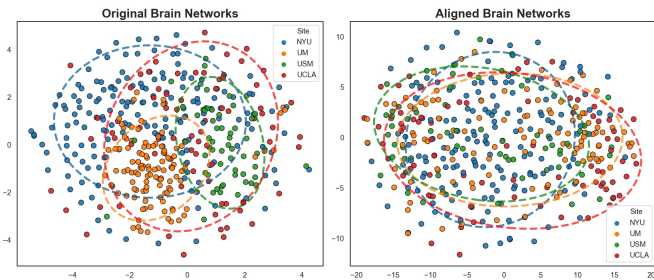


Fig. 5. Visualization of multi-site data distribution for the original and aligned brain networks in a 2D space via t-SNE. Each point represents a brain network and different colors indicate different sites. To provide a more intuitive observation of the distribution variation for different sites, we draw ellipses for the 4 sites.

+1.68%), specificity (SPE, +2.52%), and F1-score (+0.17%). These improvements highlight the robustness and effectiveness of our baseline approach. This experimental evidence provides strong support for the reliability and utility of our baseline model in addressing the classification task effectively.

D. Ablation Experiment

To validate the effectiveness of the proposed domain alignment constraints, we conducted an ablation study on the corresponding loss functions. Specifically, we selected NYU as the target domain and successively removed each domain alignment loss constraint. The experimental results are presented in Table V. The results indicate that the model's performance significantly degrades when any domain alignment loss constraint is omitted, with accuracy dropping by 6.44% in the absence of all constraints. Furthermore, the sequential removal of the four loss terms reveals a consistent decline in performance, with the removal of the prototype alignment loss and HMMD Loss3 resulting in particularly pronounced decreases. These findings demonstrate the effectiveness of the proposed domain alignment constraints in enhancing model performance.

V. DISCUSSION

In this section, we provide a detailed discussion on the impact of functional gradient components and the number of clustered communities on the model's performance. Additionally, we explore the interpretability of the model and analyze the pathological mechanisms identified by the model.

A. The influence of the hyperparameters settings on the model performance

The selection of functional gradient components and the number of clustered communities in the model ($N_{gra}=2, k=7$) was based on prior experience [37]. However, to ensure that this configuration is both reasonable and effective for the given problem, we conducted a hyperparameter search experiment by exploring different combinations of these parameters. Specifically, we searched for the number of functional gradient components N_{gra} within the range [2, 3, 4, 5] and the number of communities k within the range [5, 6, 7, 8, 9, 10]. The results of this search are presented in Figure 6.

From the results shown in Figure 6, we can conclude that selecting the first two gradient components and seven communities for constructing the community network yields the best performance. The reason for the superior performance of the first two gradient components is consistent with the findings of [33], which highlighted that the first two gradient components account for the majority of variance in the functional connectivity matrix and possess relatively clear physiological significance.

B. Interpretability

The results of the community networks obtained through clustering are visually presented in Figure 7. Through the clustering results, we observe that Community 1 is primarily concentrated in the occipital lobe, which aligns closely with the visual network [61]. This network is primarily involved in the processing of visual information. The majority of the brain regions in Community 2 are directly or indirectly involved in the control network, particularly in decision-making, executive control, emotional regulation, and cognitive tasks. For example, regions such as the middle frontal gyrus, insula, and supplementary motor area are directly engaged in cognitive and behavioral control. Meanwhile, areas like the hippocampus and amygdala are more involved in emotional regulation and memory processes, although they also influence control network activities [62]. Community 4 is predominantly associated with motor control and sensory information processing functions. Community 5 largely overlaps with the default mode network (DMN), which is fundamentally associated with cognitive processes such as introspection, self-reflection, social cognition, and memory recall [63]. Community 6 aligns with the dorsal attention network (DAN), whose activity is typically

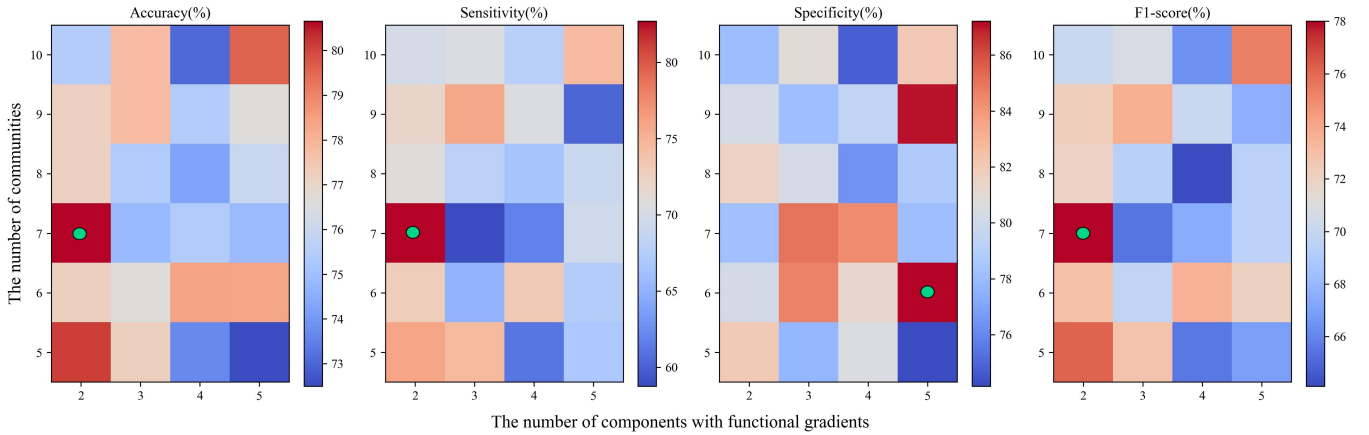


Fig. 6. The averaged four metrics obtained by different combination of k and N_{gra} . The highest value for each metric is highlighted with a green circle.

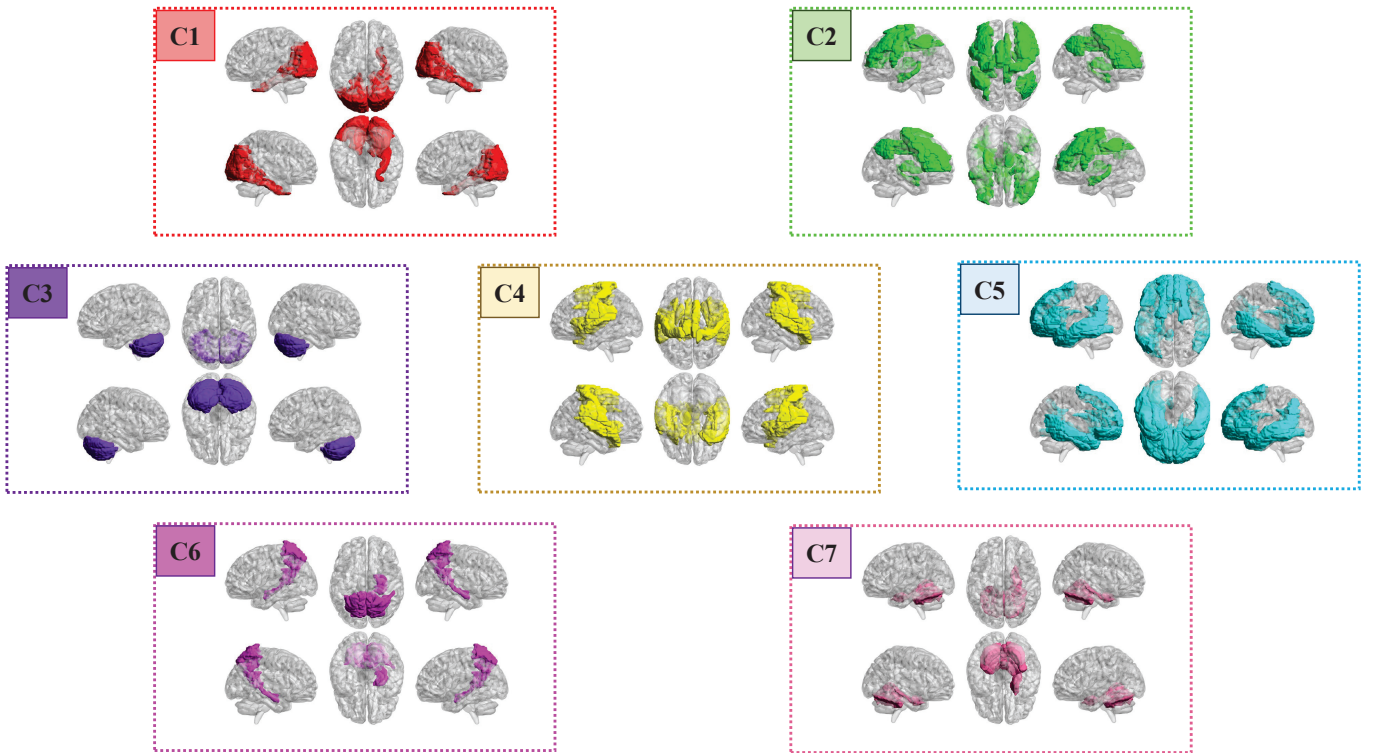


Fig. 7. Visualization of the community network results obtained through clustering.

linked with an individual's state of awareness, emotional regulation, and perception of the external world [64]. Communities 3 and 7 primarily consist of the cerebellar hemispheres and the cerebellar vermis, which together form the cerebellum. These regions are crucial for motor control, coordination, and fine-tuning of movements.

In conclusion, the identified communities are consistent with known brain networks, providing insights into the specific roles of these networks in various cognitive, sensory, and motor functions. The relationship between brain regions within

these communities reflects their specialized roles in higher-order cognitive processes and emotional regulation.

Additionally, we visualized the attention matrix of the community adjacency matrix for the network described in (17). To ensure the reliability and stability of the results, we averaged the attention matrices M_c across all folds when using the NYU site as the target domain. Furthermore, we observed that the results for the other three sites as target domains closely resembled those of NYU. Therefore, we present only the visualized attention matrix for the community network

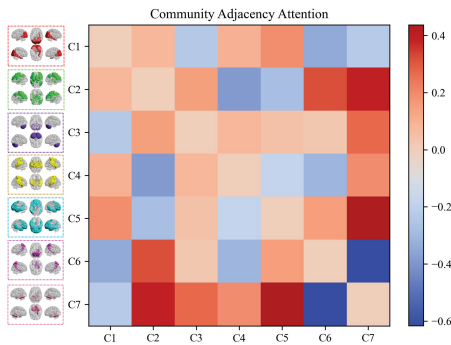


Fig. 8. Visualization of the attention mask for the adjacency matrix between communities.

adjacency matrix when NYU serves as the target domain, as shown in Figure 8.

In this attention weight matrix, values closer to zero indicate weaker connections between two communities. Upon examining the visualization, it is evident that Community 7 exhibits relatively strong attention weights (whether positive or negative) with other communities. This observation aligns well with existing findings [65], [66], which suggest that the cerebellum plays a crucial role in regulating brain function and has significant associations with ASD.

C. Limitations and Future Work

Several limitations should be addressed in future work. First, our model was evaluated on data from four sites for a single disorder, limiting its applicability to other disorders and broader datasets across additional sites. Second, we focused solely on unimodal imaging data, without exploring experiments using multimodal imaging. Extensive research [67], [68] has demonstrated that multimodal data can facilitate more efficient diagnoses and improve the identification of abnormal brain connectivity associated with neurological disorders.

In future studies, we aim to incorporate datasets from diverse psychiatric disorders and additional sites to evaluate the generalization and robustness of our method. Furthermore, we plan to leverage multimodal imaging data to enable more comprehensive diagnosis and analysis of brain disorders.

VI. CONCLUSION

In this paper, we propose a Hierarchical Multi-Site Domain Alignment method on the Hyperbolic space (H^2 MSDA) for multi-site ASD diagnosis. Specifically, our method offers the following strengths: 1. We perform feature learning in hyperbolic space and employ prototype-based learning within this space to enable accurate predictions. 2. We introduce a Hyperbolic space-adapted Maximum Mean Discrepancy to constrain the marginal distribution. 3. We propose prototype alignment, which aligns class prototypes between the target and source domains to constrain the conditional distribution effectively. Extensive experiments demonstrate the efficacy of the proposed method.

REFERENCES

- [1] V. Pandolfi, C. I. Magyar, and C. A. Dill, "Screening for autism spectrum disorder in children with down syndrome: An evaluation of the pervasive developmental disorder in mental retardation scale," *Journal of Intellectual & Developmental Disability*, vol. 43, no. 1, pp. 61–72, 2018.
- [2] R. Vohra, S. Madhavan, and U. Sambamoorthi, "Comorbidity prevalence, healthcare utilization, and expenditures of medicaid enrolled adults with autism spectrum disorders," *Autism*, vol. 21, no. 8, pp. 995–1009, 2017.
- [3] C. Lord, M. Elsabbagh, G. Baird, and J. Veenstra-Vanderweele, "Autism spectrum disorder," *The lancet*, vol. 392, no. 10146, pp. 508–520, 2018.
- [4] T. Hirota and B. H. King, "Autism spectrum disorder: A review," *Jama*, vol. 329, no. 2, pp. 157–168, 2023.
- [5] P. M. Matthews and P. Jezzard, "Functional magnetic resonance imaging," *Journal of Neurology, Neurosurgery & Psychiatry*, vol. 75, no. 1, pp. 6–12, 2004.
- [6] K. J. Friston, P. Jezzard, and R. Turner, "Analysis of functional mri time-series," *Human brain mapping*, vol. 1, no. 2, pp. 153–171, 1994.
- [7] D. Dong, C. Luo, X. Guell, Y. Wang, H. He, M. Duan, S. B. Eickhoff, and D. Yao, "Compression of cerebellar functional gradients in schizophrenia," *Schizophrenia bulletin*, vol. 46, no. 5, pp. 1282–1295, 2020.
- [8] A. I. Luppi, P. A. Mediano, F. E. Rosas, N. Holland, T. D. Fryer, J. T. O'Brien, J. B. Rowe, D. K. Menon, D. Bor, and E. A. Stamatakis, "A synergistic core for human brain evolution and cognition," *Nature Neuroscience*, vol. 25, no. 6, pp. 771–782, 2022.
- [9] C. Dong and D. Sun, "Brain network classification based on dynamic graph attention information bottleneck," *Computer Methods and Programs in Biomedicine*, vol. 243, p. 107913, 2024.
- [10] Y. Wang, S. Genon, D. Dong, F. Zhou, C. Li, D. Yu, K. Yuan, Q. He, J. Qiu, T. Feng *et al.*, "Covariance patterns between sleep health domains and distributed intrinsic functional connectivity," *Nature Communications*, vol. 14, no. 1, p. 7133, 2023.
- [11] R. Song, P. Cao, G. Wen, P. Zhao, Z. Huang, X. Zhang, J. Yang, and O. R. Zaiane, "BrainDas: Structure-aware domain adaptation network for multi-site brain network analysis," *Medical Image Analysis*, vol. 96, p. 103211, 2024. [Online]. Available: <https://www.sciencedirect.com/science/article/pii/S1361841524001361>
- [12] Y. Fang, J. Wu, Q. Wang, S. Qiu, A. Bozoki, and M. Liu, "Source-free collaborative domain adaptation via multi-perspective feature enrichment for functional mri analysis," *Pattern Recognition*, vol. 157, p. 110912, 2025. [Online]. Available: <https://www.sciencedirect.com/science/article/pii/S0031320324006630>
- [13] W. M. Kouw and M. Loog, "A review of domain adaptation without target labels," *IEEE Transactions on Pattern Analysis and Machine Intelligence*, vol. 43, no. 3, pp. 766–785, 2021.
- [14] S. Zhao, X. Yue, S. Zhang, B. Li, H. Zhao, B. Wu, R. Krishna, J. E. Gonzalez, A. L. Sangiovanni-Vincentelli, S. A. Seshia, and K. Keutzer, "A review of single-source deep unsupervised visual domain adaptation," *IEEE Transactions on Neural Networks and Learning Systems*, vol. 33, no. 2, pp. 473–493, 2022.
- [15] S. Sun, H. Shi, and Y. Wu, "A survey of multi-source domain adaptation," *Information Fusion*, vol. 24, pp. 84–92, 2015. [Online]. Available: <https://www.sciencedirect.com/science/article/pii/S1566253514001316>
- [16] Y. Chu, H. Ren, L. Qiao, and M. Liu, "Resting-state functional mri adaptation with attention graph convolution network for brain disorder identification," *Brain Sciences*, vol. 12, no. 10, p. 1413, 2022.
- [17] B. Sun and K. Saenko, "Deep coral: Correlation alignment for deep domain adaptation," in *Computer Vision—ECCV 2016 Workshops: Amsterdam, The Netherlands, October 8–10 and 15–16, 2016, Proceedings, Part III 14*. Springer, 2016, pp. 443–450.
- [18] Y. Fang, M. Wang, G. G. Potter, and M. Liu, "Unsupervised cross-domain functional mri adaptation for automated major depressive disorder identification," *Medical Image Analysis*, vol. 84, p. 102707, 2023. [Online]. Available: <https://www.sciencedirect.com/science/article/pii/S1361841522003358>
- [19] A. Gretton, K. Borgwardt, M. Rasch, B. Schölkopf, and A. Smola, "A kernel method for the two-sample-problem," in *Advances in Neural Information Processing Systems*, B. Schölkopf, J. Platt, and T. Hoffman, Eds., vol. 19. MIT Press, 2006. [Online]. Available: https://proceedings.neurips.cc/paper_files/paper/2006/file/e9fb2eda3d9c55a0d89c98d6c54b5b3e-Paper.pdf

- [20] X. Li, Y. Gu, N. Dvornek, L. H. Staib, P. Ventola, and J. S. Duncan, "Multi-site fmri analysis using privacy-preserving federated learning and domain adaptation: Abide results," *Medical Image Analysis*, vol. 65, p. 101765, 2020. [Online]. Available: <https://www.sciencedirect.com/science/article/pii/S1361841520301298>
- [21] Y. Ganin, E. Ustinova, H. Ajakan, P. Germain, H. Larochelle, F. Laviolette, M. March, and V. Lempitsky, "Domain-adversarial training of neural networks," *Journal of Machine Learning Research*, vol. 17, no. 59, pp. 1–35, 2016. [Online]. Available: <http://jmlr.org/papers/v17/15-239.html>
- [22] S. Masoudnia and R. Ebrahimpour, "Mixture of experts: a literature survey," *Artificial Intelligence Review*, vol. 42, pp. 275–293, 2014.
- [23] X. Liu, J. Wu, W. Li, Q. Liu, L. Tian, and H. Huang, "Domain adaptation via low rank and class discriminative representation for autism spectrum disorder identification: A multi-site fmri study," *IEEE Transactions on Neural Systems and Rehabilitation Engineering*, vol. 31, pp. 806–817, 2023.
- [24] M. Yang, H. Verma, D. C. Zhang, J. Liu, I. King, and R. Ying, "Hypformer: Exploring efficient transformer fully in hyperbolic space," in *Proceedings of the 30th ACM SIGKDD Conference on Knowledge Discovery and Data Mining*, 2024, pp. 3770–3781.
- [25] X. Gu, J. Sun, and Z. Xu, "Unsupervised and semi-supervised robust spherical space domain adaptation," *IEEE Transactions on Pattern Analysis and Machine Intelligence*, vol. 46, no. 3, pp. 1757–1774, 2024.
- [26] M. Yang, M. Zhou, H. Xiong, and I. King, "Hyperbolic temporal network embedding," *IEEE Transactions on Knowledge and Data Engineering*, vol. 35, no. 11, pp. 11 489–11 502, 2023.
- [27] J. Dai, Y. Wu, Z. Gao, and Y. Jia, "A hyperbolic-to-hyperbolic graph convolutional network," in *Proceedings of the IEEE/CVF Conference on Computer Vision and Pattern Recognition (CVPR)*, June 2021, pp. 154–163.
- [28] M. Nickel and D. Kiela, "Poincaré embeddings for learning hierarchical representations," in *Advances in Neural Information Processing Systems*, I. Guyon, U. V. Luxburg, S. Bengio, H. Wallach, R. Fergus, S. Vishwanathan, and R. Garnett, Eds., vol. 30. Curran Associates, Inc., 2017. [Online]. Available: https://proceedings.neurips.cc/paper_files/paper/2017/file/59dfa2df42d9e3d41f5b02bfc32229dd-Paper.pdf
- [29] C. Baker, I. Suárez-Méndez, G. Smith, E. B. Marsh, M. Funke, J. C. Mosher, F. Maestú, M. Xu, and D. Pantazis, "Hyperbolic graph embedding of meg brain networks to study brain alterations in individuals with subjective cognitive decline," *IEEE Journal of Biomedical and Health Informatics*, vol. 28, no. 12, pp. 7357–7368, 2024.
- [30] X. Guell, J. D. Schmahmann, J. D. Gabrieli, and S. S. Ghosh, "Functional gradients of the cerebellum," *elife*, vol. 7, p. e36652, 2018.
- [31] J. M. Huntenburg, P.-L. Bazin, and D. S. Margulies, "Large-scale gradients in human cortical organization," *Trends in cognitive sciences*, vol. 22, no. 1, pp. 21–31, 2018.
- [32] S. Guo, L. Feng, R. Ding, S. Long, H. Yang, X. Gong, J. Lu, and D. Yao, "Functional gradients in prefrontal regions and somatomotor networks reflect the effect of music training experience on cognitive aging," *Cerebral Cortex*, vol. 33, no. 12, pp. 7506–7517, 2023.
- [33] Z.-Q. Gong and X.-N. Zuo, "Connectivity gradients in spontaneous brain activity at multiple frequency bands," *Cerebral Cortex*, vol. 33, no. 17, pp. 9718–9728, 2023.
- [34] S.-J. Hong, R. Vos de Wael, R. A. Bethlehem, S. Larivière, C. Paquola, S. L. Valk, M. P. Milham, A. Di Martino, D. S. Margulies, J. Smallwood *et al.*, "Atypical functional connectome hierarchy in autism," *Nature communications*, vol. 10, no. 1, p. 1022, 2019.
- [35] S. G. Urchs, A. Tam, P. Orban, C. Moreau, Y. Benhajali, H. D. Nguyen, A. C. Evans, and P. Bellec, "Functional connectivity subtypes associate robustly with asd diagnosis," *Elife*, vol. 11, p. e56257, 2022.
- [36] A. Di Martino, C.-G. Yan, Q. Li, E. Denio, F. X. Castellanos, K. Alaerts, J. S. Anderson, M. Assaf, S. Y. Bookheimer, M. Dapretto *et al.*, "The autism brain imaging data exchange: towards a large-scale evaluation of the intrinsic brain architecture in autism," *Molecular psychiatry*, vol. 19, no. 6, pp. 659–667, 2014.
- [37] Y. Luo, Q. Chen, F. Li, L. Yi, P. Xu, and Y. Zhang, "Hierarchical feature extraction on functional brain networks for autism spectrum disorder identification with resting-state fmri data," *arXiv preprint arXiv:2412.02424*, 2024.
- [38] R. Vos de Wael, O. Benkarim, C. Paquola, S. Larivière, J. Royer, S. Tavakol, T. Xu, S.-J. Hong, G. Langs, S. Valk *et al.*, "Brainspace: a toolbox for the analysis of macroscale gradients in neuroimaging and connectomics datasets," *Communications biology*, vol. 3, no. 1, p. 103, 2020.
- [39] C. Yan and Y. Zang, "Dparfs: a matlab toolbox for" pipeline" data analysis of resting-state fmri," *Frontiers in systems neuroscience*, vol. 4, p. 1377, 2010.
- [40] N. Tzourio-Mazoyer, B. Landeau, D. Papathanassiou, F. Crivello, O. Etard, N. Delcroix, B. Mazoyer, and M. Joliot, "Automated anatomical labeling of activations in spm using a macroscopic anatomical parcellation of the mni mri single-subject brain," *Neuroimage*, vol. 15, no. 1, pp. 273–289, 2002.
- [41] M. A. Rodríguez-Flores and F. Papadopoulos, "Hyperbolic mapping of human proximity networks," *Scientific reports*, vol. 10, no. 1, p. 20244, 2020.
- [42] W. Tong, Y.-X. Li, X.-Y. Zhao, Q.-Q. Chen, Y.-B. Gao, P. Li, and E. Q. Wu, "fmri-based brain disease diagnosis: A graph network approach," *IEEE Transactions on Medical Robotics and Bionics*, vol. 5, no. 2, pp. 312–322, 2023.
- [43] X. Liao, M. Cao, M. Xia, and Y. He, "Individual differences and time-varying features of modular brain architecture," *NeuroImage*, vol. 152, pp. 94–107, 2017. [Online]. Available: <https://www.sciencedirect.com/science/article/pii/S1053811917301775>
- [44] O. Sporns and R. F. Betzel, "Modular brain networks," *Annual review of psychology*, vol. 67, no. 1, pp. 613–640, 2016.
- [45] M. P. Van Den Heuvel, R. C. Mandl, R. S. Kahn, and H. E. Hulshoff Pol, "Functionally linked resting-state networks reflect the underlying structural connectivity architecture of the human brain," *Human brain mapping*, vol. 30, no. 10, pp. 3127–3141, 2009.
- [46] M. P. Van Den Heuvel and H. E. H. Pol, "Exploring the brain network: a review on resting-state fmri functional connectivity," *European neuropsychopharmacology*, vol. 20, no. 8, pp. 519–534, 2010.
- [47] L. Geerligs, M. Rubinov, R. N. Henson *et al.*, "State and trait components of functional connectivity: individual differences vary with mental state," *Journal of Neuroscience*, vol. 35, no. 41, pp. 13 949–13 961, 2015.
- [48] E. Canario, D. Chen, and B. Biswal, "A review of resting-state fmri and its use to examine psychiatric disorders," *Psychoradiology*, vol. 1, no. 1, pp. 42–53, 2021.
- [49] C. L. Gallen and M. D'Esposito, "Brain modularity: a biomarker of intervention-related plasticity," *Trends in cognitive sciences*, vol. 23, no. 4, pp. 293–304, 2019.
- [50] Q. Wang, W. Wang, Y. Fang, P.-T. Yap, H. Zhu, H.-J. Li, L. Qiao, and M. Liu, "Leveraging brain modularity prior for interpretable representation learning of fmri," *IEEE Transactions on Biomedical Engineering*, vol. 71, no. 8, pp. 2391–2401, 2024.
- [51] Y. Ding, N. Robinson, C. Tong, Q. Zeng, and C. Guan, "Lggnnet: Learning from local-global-graph representations for brain-computer interface," *IEEE Transactions on Neural Networks and Learning Systems*, vol. 35, no. 7, pp. 9773–9786, 2024.
- [52] H. Yan, Z. Li, Q. Wang, P. Li, Y. Xu, and W. Zuo, "Weighted and class-specific maximum mean discrepancy for unsupervised domain adaptation," *IEEE Transactions on Multimedia*, vol. 22, no. 9, pp. 2420–2433, 2020.
- [53] L. Tang, Q. Zhang, J. Xuan, T. Shi, and R. Li, "Multitarget domain adaptation with transferable hyperbolic prototypes for intelligent fault diagnosis," *Knowledge-Based Systems*, vol. 257, p. 109952, 2022. [Online]. Available: <https://www.sciencedirect.com/science/article/pii/S0950705122010450>
- [54] J. Zhang, P. Wan, and D. Zhang, "Transport-based joint distribution alignment for multi-site autism spectrum disorder diagnosis using resting-state fmri," in *Medical Image Computing and Computer Assisted Intervention—MICCAI 2020: 23rd International Conference, Lima, Peru, October 4–8, 2020, Proceedings, Part II 23*. Springer, 2020, pp. 444–453.
- [55] M. Wang, D. Zhang, J. Huang, P.-T. Yap, D. Shen, and M. Liu, "Identifying autism spectrum disorder with multi-site fmri via low-rank domain adaptation," *IEEE Transactions on Medical Imaging*, vol. 39, no. 3, pp. 644–655, 2020.
- [56] M. Kunda, S. Zhou, G. Gong, and H. Lu, "Improving multi-site autism classification via site-dependence minimization and second-order functional connectivity," *IEEE Transactions on Medical Imaging*, vol. 42, no. 1, pp. 55–65, 2023.
- [57] H. Jiang, P. Cao, M. Xu, J. Yang, and O. Zaiane, "Hi-gcn: A hierarchical graph convolution network for graph embedding learning of brain network and brain disorders prediction," *Computers in Biology and Medicine*, vol. 127, p. 104096, 2020.
- [58] J. Kawahara, C. J. Brown, S. P. Miller, B. G. Booth, V. Chau, R. E. Grunau, J. G. Zwicker, and G. Hamarneh, "Brainnetcn: Convolutional neural networks for brain networks; towards predicting neurodevelopment," *NeuroImage*, vol. 146, pp. 1038–1049, 2017.
- [59] G. Wen, P. Cao, H. Bao, W. Yang, T. Zheng, and O. Zaiane, "Mvs-gcn: A prior brain structure learning-guided multi-view graph convolution

- network for autism spectrum disorder diagnosis,” *Computers in biology and medicine*, vol. 142, p. 105239, 2022.
- [60] Y. Luo, N. Li, Y. Pan, W. Qiu, L. Xiong, and Y. Zhang, “Aided diagnosis of autism spectrum disorder based on a mixed neural network model,” in *International Conference on Neural Information Processing*. Springer, 2023, pp. 150–161.
- [61] M. Lee, C. Smyser, and J. Shimony, “Resting-state fmri: A review of methods and clinical applications,” *American Journal of Neuroradiology*, vol. 34, no. 10, pp. 1866–1872, 2013. [Online]. Available: <http://www.ajnr.org/content/34/10/1866>
- [62] J. M. Chein and W. Schneider, “Neuroimaging studies of practice-related change: fmri and meta-analytic evidence of a domain-general control network for learning,” *Cognitive Brain Research*, vol. 25, no. 3, pp. 607–623, 2005.
- [63] M. E. Raichle, A. M. MacLeod, A. Z. Snyder, W. J. Powers, D. A. Gusnard, and G. L. Shulman, “A default mode of brain function,” *Proceedings of the national academy of sciences*, vol. 98, no. 2, pp. 676–682, 2001.
- [64] M. Corbetta and G. L. Shulman, “Control of goal-directed and stimulus-driven attention in the brain,” *Nature reviews neuroscience*, vol. 3, no. 3, pp. 201–215, 2002.
- [65] M. W. Mosconi, Z. Wang, L. M. Schmitt, P. Tsai, and J. A. Sweeney, “The role of cerebellar circuitry alterations in the pathophysiology of autism spectrum disorders,” *Frontiers in neuroscience*, vol. 9, p. 156522, 2015.
- [66] D. R. Hampson and G. J. Blatt, “Autism spectrum disorders and neuropathology of the cerebellum,” *Frontiers in neuroscience*, vol. 9, p. 420, 2015.
- [67] X. Xu, T. Wang, W. Li, H. Li, B. Xu, M. Zhang, L. Yue, P. Wang, and S. Xiao, “Morphological, structural, and functional networks highlight the role of the cortical-subcortical circuit in individuals with subjective cognitive decline,” *Frontiers in Aging Neuroscience*, vol. 13, p. 688113, 2021.
- [68] L. Wei, B. Liu, J. He, M. Zhang, and Y. Huang, “Autistic spectrum disorders diagnose with graph neural networks,” in *Proceedings of the 31st ACM International Conference on Multimedia*, ser. MM '23. New York, NY, USA: Association for Computing Machinery, 2023, p. 8819–8827. [Online]. Available: <https://doi.org/10.1145/3581783.3613818>



First A. Author (Fellow, IEEE) and all authors may include biographies. Biographies are often not included in conference-related papers. This author is an IEEE Fellow. The first paragraph may contain a place and/or date of birth (list place, then date). Next, the author’s educational background is listed. The degrees should be listed with type of degree in what field, which institution, city, state, and country, and year the degree was earned. The author’s major field of study should be lower-cased.

The second paragraph uses the pronoun of the person (he or she) and not the author’s last name. It lists military and work experience, including summer and fellowship jobs. Job titles are capitalized. The current job must have a location; previous positions may be listed without one. Information concerning previous publications may be included. Try not to list more than three books or published articles. The format for listing publishers of a book within the biography is: title of book (publisher name, year) similar to a reference. Current and previous research interests end the paragraph.

The third paragraph begins with the author’s title and last name (e.g., Dr. Smith, Prof. Jones, Mr. Kajor, Ms. Hunter). List any memberships in professional societies other than the IEEE. Finally, list any awards and work for IEEE committees and publications. If a photograph is provided, it should be of good quality, and professional-looking.